HIGH-n STABILITY OF ALPHA PARTICLE DRIVEN ALFVÉN EIGENMODES

G. VLAD, F. ZONCA, F. ROMANELLI
Associazione Euratom–ENEA sulla Fusione,
C.R.E. Frascati, Frascati, Rome, Italy

ABSTRACT. In the present work, we analyse the two dimensional (2-D) mode structures and global stability of the Alfvén branches, whose frequencies are close to the toroidicity induced Alfvén continuum gap. The fully 2-D problem is solved using a two spatial-scale WKBJ formalism without employing perturbation theory in treating drive and damping terms. A code that solves the 2-D mode structures and global stability of the Alfvén branches is presented. Applications to a model toroidal equilibrium with ITER relevant plasma parameters are analysed. Results indicate that no unstable modes are present in the considered reference scenario.

1. INTRODUCTION

In the gap of the shear Alfvén continuous spectrum, produced by the toroidicity induced poloidal variation of the plasma equilibrium [1], discrete modes can exist, called toroidal Alfvén eigenmodes (TAEs) [2], which can be destabilized by the resonant interaction with alpha particles. For typical parameters of an ignition experiment, in fact, the Alfvén frequency is of the order of the alpha particle transit frequency [3].

The TAE stability is a result of competition among several effects. The transit resonance with the bulk ions plays a strongly stabilizing role in the plasma core [4]. Meanwhile, trapped electron collisional effects [5, 6] may be important in the outer part of the discharge. The alpha particle drive is localized around the region of the maximum alpha pressure gradient. Thus, the mode stability strongly depends on the radial mode localization which can be determined only by solving a fully two dimensional (2-D) problem. Furthermore, for realistic parameters, the effect of the drive and damping terms cannot be treated perturbatively but should be considered at the same order as that at which toroidicity enters [7–9]. Finite orbit widths of energetic particles [7–12] as well as bulk ion finite Larmor radius effects [9, 13–15] also need to be accounted for. The aim of the present paper is to present a non-perturbative, fully 2-D analysis of gap mode stability [8, 9]. Applications to ITER-like equilibria will also be discussed. A preliminary investigation of this problem, using perturbation theory in the drive and damping terms, has been presented in Ref. [16]. A comparison between the results presented here and those derived previously [16] will serve the purpose of estimating the importance of non-perturbative analyses of energetic particle dynamics and of bulk-ion kinetic effects.

Since the most unstable modes correspond to moderately high toroidal numbers n, the mode stability can be properly addressed in the context of a 2-D WKBJ formalism. Within this theoretical framework, the global mode structure corresponds to the superposition of poloidal harmonics with similar shape, modulated by a global envelope $A(r)$. The eigenvalue problem is solved in two steps: at the first step the form of each harmonic is determined; then, the structure of the global envelope is found. A generic harmonic with poloidal number m is characterized by a two scale structure, namely a typical scale of the order a/m far from the gap location (a being the plasma minor radius), and a typical scale $\epsilon a/m$ in the gap region ($\epsilon \equiv a/R_0$, R_0 being the plasma major radius). The two scale nature of each harmonic is a consequence of the narrowness of the gap induced by toroidal effects. The function $A(r)$ is determined at the next order in the two scale-lengths WKBJ approach, by considering the radial variation of the equilibrium profiles. It has been shown [17–19] that the width of the global envelope is of the order of ϵa. Thus, TAEs have the character of a global instability also at high n.

The plan of the paper is the following. In Section 2 the general form of the dispersion relation is presented. In Section 3 the numerical code for the solution of the radial mode problem is discussed. Applications to the stability on ITER-like equilibria are presented in Section 4. Concluding remarks are given in Section 5.

2. LOCAL DISPERSION FUNCTION

A circular flux surfaces tokamak equilibrium, described by the conventional (s, α) model [20], with $s \equiv rq'/q$ the magnetic shear and $\alpha \equiv -Rq^2\beta'$, is considered here.

In the high-n limit, the fluctuating scalar potential can be represented as [17–19]

$$\delta\phi(t; r, \vartheta, \varphi) = \mathcal{A}(\tau)\mathrm{e}^{-\mathrm{i}\omega t + \mathrm{i}n\varphi} \sum_m \phi(\tau, \tau - m)\mathrm{e}^{-\mathrm{i}m\vartheta} \tag{1}$$

where $\tau \equiv nq$ is a dimensionless radial 'flux' co-ordinate, $\phi(\tau, \tau - m)$ is a 'shape function' accounting for fast (compared with equilibrium) radial variation of the eigenmode structure at $\tau - m \simeq \pm 1/2$, and $\mathcal{A}(\tau)$ is given by the WKBJ expression [17–19],

$$\mathcal{A}(\tau) = \frac{K \exp\left(\mathrm{i}\int^{\tau} \theta_k(\tau')\,\mathrm{d}\tau'\right)}{\sqrt{(1/nq')\partial F/\partial\theta_k}} \tag{2}$$

Here, K is an arbitrary constant and the WKBJ phase $\theta_k(\tau)$ is implicitly defined by the local dispersion relation

$$F(\omega; \tau, \theta_k) = 0$$

expressed in terms of the local dispersion function $F(\omega; \tau, \theta_k)$ (cf. later in this section).

Using the Fourier conjugate representation for the scalar potential $\phi(\tau, \tau - m)$ [17–19]

$$\phi(\tau, \tau - m) = \int_{-\infty}^{+\infty} \mathrm{d}\theta\, \mathrm{e}^{-\mathrm{i}(\tau - m)\theta}\Phi(\tau, \theta) \tag{3}$$

the general form for the local dispersion function of toroidal Alfvén modes can be derived by solving the following vorticity equation with homogeneous boundary conditions [3, 8, 9, 15]:

$$\left(\partial_\theta^2 + \Omega^2(1 + 2\epsilon_0\cos\theta) + \frac{\alpha\cos\theta}{p} - \frac{(s - \alpha\cos\theta)^2}{p^2} - \frac{s^4\rho_{\mathrm{K}}^2}{p}(\theta - \theta_k)^4\right)\hat{\Phi} - \sum_j \frac{q^2R^2}{k_\vartheta^2}\frac{\eta_j}{p^{1/2}}\langle\omega_{\mathrm{d}}J_0(\lambda_\rho)\delta G\rangle_j = 0 \tag{4}$$

Here, $\hat{\Phi} = p^{1/2}\Phi$, $p(\theta) = 1 + [s(\theta - \theta_k) - \alpha\sin\theta]^2$, $\Omega^2 = \omega^2/\omega_{\mathrm{A}}^2$, $\omega_{\mathrm{A}} = v_{\mathrm{A}}/qR$, v_{A} is the Alfvén speed, $\epsilon_0 = 2(r/R_0 + \Delta')$, $k_\vartheta \equiv nq/r$ and Δ' is the derivative of the Shafranov shift.

In Eq. (4),

$$\rho_{\mathrm{K}}^2 = (k_\vartheta^2\rho_{\mathrm{Li}}^2/4)[3/4 + (T_{\mathrm{e}}/T_{\mathrm{i}})(1 - \mathrm{i}\delta)] - \mathrm{i}k_\vartheta^2c^2\eta/16\pi\omega$$

accounts for the kinetic effects associated with finite ion Larmor orbits and parallel electron dynamics: ρ_{Li} is the ion Larmor radius, η is the plasma resistivity entering the parallel Ohm's law, while δ describes other dissipative effects associated, for example, with collisions with trapped electrons [5, 6] or, if properly modelled, also the usual Landau collisionless dissipation. Typically, the most important dissipation mechanism related to the electron dynamics is the trapped electron collisional damping [6]. Therefore, for δ we use the following form [14]:

$$\delta = \frac{\epsilon_0^{3/2}}{\epsilon_0^{3/2} + (\nu_{\mathrm{e}}/\omega)^{3/2}}\sqrt{\frac{\nu_{\mathrm{e}}}{\omega}}\left[1.4 + \frac{1}{4}\ln\left(1 + \epsilon_0\frac{\omega}{\nu_{\mathrm{e}}}\right)\right]^{-3/2} \tag{5}$$

Here, $\nu_{\mathrm{e}} = 4\pi e^4 n_{\mathrm{e}} \ln\Lambda/[m_{\mathrm{e}}^{1/2}(2T_{\mathrm{e}})^{3/2}]$, with $\ln\Lambda$ being the Coulomb logarithm.

The summation in Eq. (4) is over the species and accounts for the resonant interaction of the mode with the particle magnetic drifts. Hence, it includes the energetic particle drive and electron and ion 'drift' Landau damping. Note that J_0 is the Bessel function of the first kind and zero index, with argument

$$\lambda_{\rho_j} = k_\perp(m_jc/e_jB)v_\perp, \quad k_\perp^2 = k_\vartheta^2 + k_r^2, \quad \eta_j = 4\pi\omega e_j/c^2, \quad \omega_{\mathrm{d}j}(\theta) = \Omega_{\mathrm{d}j}g(\theta),$$

$$g(\theta) = \cos\theta + [s(\theta - \theta_k) - \alpha\sin\theta]\sin\theta, \quad \Omega_{\mathrm{d}j} = k_\vartheta cm_j(v_\perp^2/2 + v_\parallel^2)/e_jBR$$

and

$$\langle ... \rangle = \int \mathrm{d}^3 v \, (...)$$

The distribution function δG_j is derived from the gyrokinetic equation [3]

$$[\omega_t \partial_\theta - \mathrm{i}(\omega - \omega_d)]_j \, \delta G_j = \mathrm{i}\left(\frac{e}{m}\right)_j Q F_{0j} \frac{1}{p^{1/2}} \left(\frac{\omega_d}{\omega}\right)_j J_0(\lambda_{\rho_j}) \hat{\Phi} \tag{6}$$

where $\omega_t = v_\parallel / qR$ is the transit frequency, $QF_{0j} = (\omega \partial_E + \hat{\omega}_*)_j F_{0j}$, $E = v^2/2$ and $\hat{\omega}_{*j} F_{0j} = (m_j c / e_j B)(\boldsymbol{k} \times \boldsymbol{e}_\parallel) \cdot \nabla F_{0j}$.

Equations (4), with homogeneous boundary conditions, and (6), with causality constraints, define a well posed integrodifferential problem, leading to the desired general form of the local dispersion function. This problem has been solved in Refs [7–9], using asymptotic techniques. The general form of the local dispersion function for toroidal Alfvén modes, obtained in Ref. [9], is

$$\begin{aligned} F(\omega; \tau, \theta_k) = {} & Z_f [F_1 (1 + 2\delta U_{K,u}) + 2F_2 (\delta W_{K,u} + \delta W_{K,T}) - 2F_3 \delta W_{K,T}] \\ & + 2G_f [F_2 (1 + 2\delta U_{K,u}) - 2F_1 (\delta W_{K,u} + \delta W_{K,T})] \\ & + 2(H_f \cos\theta_k + L_f \sin\theta_k)[F_3 (1 + 2\delta U_{K,u}) - 2F_1 \delta W_{K,T}] \end{aligned} \tag{7}$$

In Eq. (7), Z_f, G_f, H_f and L_f are the same functions of (s, α, θ_k) defined in Eq. (53) of Ref. [18], where their numerical values were tabulated and approximate analytical estimates of them were given. Moreover,

$$\delta W_{K,u} = \frac{\pi^2}{4s} \frac{e^2}{mc^2} \frac{q^2 R_0^2}{k_\vartheta^2} \left\langle \frac{\Omega_d^2 Q F_0}{\Delta (1 + \Delta^2)^{3/2}} \left(\frac{\omega}{\omega_t^2/4 - \omega^2} + \frac{\omega}{9\omega_t^2/4 - \omega^2} \right) \right\rangle \tag{8}$$

$$\delta U_{K,u} = \frac{\pi^2}{4s} \frac{e^2}{mc^2} \frac{q^2 R_0^2}{k_\vartheta^2} \left\langle \frac{\Omega_d^2 Q F_0}{\Delta (1 + \Delta^2)^{3/2}} \left(\frac{-\mathrm{i}\omega_t/2}{\omega_t^2/4 - \omega^2} + \frac{\mathrm{i}3\omega_t/2}{9\omega_t^2/4 - \omega^2} \right) \right\rangle \tag{9}$$

$$\begin{aligned} \delta W_{K,T} = {} & \frac{2\pi^2 e^2}{mc^2} q R_0 B_0 \sum_{\sigma = \pm} \int \mathrm{d}E \int \mathrm{d}\mu \left(\frac{\Omega_d}{k_\vartheta} \right)^2 \tau_b Q F_0 \\ & \times \left(\frac{1}{\bar{\omega}_d - \omega} + \frac{\theta_b^2/8s}{\Delta_T (1 + \Delta_T^2)^{3/2}} \frac{\omega - \bar{\omega}_d}{\omega_b^2 - (\omega - \bar{\omega}_d)^2} \right) \end{aligned} \tag{10}$$

Here, $\Delta^2 = (k_\vartheta^2/4)(\rho_L^2 + \rho_d^2/2)$, $\rho_d^2 = \Omega_d^2 / k_\vartheta^2 \omega_t^2$, $\Delta_T^2 = (k_\vartheta^2/4)(\rho_L^2 + \theta_b^2 \rho_b^2/2)$, θ_b is the bounce angle for trapped particles and $\rho_b^2 = \Omega_d^2 / k_\vartheta^2 \omega_b^2$. Furthermore, a summation on all energetic particle species is implicitly assumed.

Equations (8) to (10) give the contribution of energetic particles to the mode dynamics for $\epsilon_0 \lesssim k_\vartheta \rho_E$ (here and in the following, the subscript 'E' refers to energetic particle quantities). In the longer wavelength case, $k_\vartheta \rho_E < \epsilon_0$, the usual zero orbit analysis of energetic particle dynamics applies [3], and the quantities $\delta W_{K,u}$, $\delta U_{K,u}$ and $\delta W_{K,T}$ are set to zero. The fast ion contribution, in this case, is accounted for by terms contained in the expressions for F_1, F_2 and F_3, appearing in Eq. (7) (cf. later in this section).

Equations (8) and (9) describe the well known wave–particle resonances at $v_\parallel = v_A$ and $v_\parallel = v_A/3$. The term $\delta W_{K,u}$ can be interpreted as the circulating particle contribution to the potential energy [8]. The analogous $\delta U_{K,u}$ term has a similar interpretation, with the difference that it is vanishing for particle distribution functions symmetric in $v_\parallel$. Equation (10) gives the effect of trapped energetic particles. It describes the mode resonance with the toroidal precession rate of the banana orbits $\bar{\omega}_d$ and with the bounce motion of trapped particles between magnetic mirror points at rate ω_b. Only the first bounce-resonance harmonic has been considered here, since higher resonances occur at higher mode frequencies and are usually negligible [7, 8]. In this simplified analysis, let us consider one energetic particle species only, with a slowing down equilibrium distribution function, symmetric in $v_\parallel$ and with fixed pitch angle. Considering only circulating particles, it is possible to show that $\delta U_{K,u} = \delta W_{K,T} = 0$ and that, for $\epsilon_0 \lesssim k_\vartheta \rho_E \lesssim 1$ [7, 8],

$$\delta W_{\mathrm{K,u}} \simeq \frac{\pi\alpha_{\mathrm{E}}}{\sqrt{2}s}\frac{\omega}{\omega_{\mathrm{tm}}}\sum_{\ell=1,3}\frac{1}{\ell^2}\left[1-\frac{\omega}{\ell\omega_{\mathrm{tm}}}\ln\left(\frac{2\omega+\ell\omega_{\mathrm{tm}}}{2\omega-\ell\omega_{\mathrm{tm}}}\right)\right]$$
$$+\frac{3\pi}{8}\frac{q\beta_{\mathrm{E}}}{s}\left|\frac{1}{k_\theta\rho_{\mathrm{LE,m}}}\right|\sqrt{1-\alpha_0 B_0}\sum_{\ell=1,3}\frac{\omega}{\ell\omega_{\mathrm{tm}}}\ln\left(\frac{2\omega+\ell\omega_{\mathrm{tm}}}{2\omega-\ell\omega_{\mathrm{tm}}}\right) \tag{11}$$

Here, $\alpha_{\mathrm{E}} = -R_0 q^2 \beta'_{\mathrm{E}}$, $\alpha_0 = v_\perp^2/[B_0(v_\parallel^2+v_\perp^2)]$, $\rho_{\mathrm{LE,m}} = E_{\mathrm{m}}^{1/2}/\omega_{\mathrm{cE}}$ and ω_{tm} are, respectively, the Larmor radius and the transit frequency at the maximum fast particle energy. Equation (11) is independent of the mode number, as expected for the most unstable wavelengths, in the range $\epsilon_0 \lesssim k_\vartheta\rho_{\mathrm{E}} \lesssim 1$ [7–12], and it describes the resonant mode interaction with the energetic ions at $\omega \simeq \omega_{\mathrm{tm}}/2$ and $\omega \simeq 3\omega_{\mathrm{tm}}/2$.

The functions F_1, F_2 and F_3 in Eq. (7) are determined from the large-θ solution of Eq. (4), and they depend on the parameters $\hat{\Gamma}_\pm$, Δ_{K} and β_2, where $\Delta_{\mathrm{K}} \equiv s^2\rho_{\mathrm{K}}^2/(\epsilon_0\Omega^2)^3$, $\hat{\Gamma}_\pm = (\Omega^2 - 1/4)/\epsilon_0\Omega^2 \pm 1 - \beta_1$ and [3]

$$\beta_1 = \frac{\pi q^2}{\epsilon_0\Omega^2 B^2}\sum_j m_j\left(\frac{v_\perp^2}{2}+v_\parallel^2\right)^2 QF_{0j}\left(\frac{\omega}{\omega_{\mathrm{t}}^2/4-\omega^2}+\frac{\omega}{9\omega_{\mathrm{t}}^2/4-\omega^2}\right)_j \tag{12a}$$

$$\beta_2 = \frac{\pi q^2}{\epsilon_0\Omega^2 B^2}\sum_j m_j\left(\frac{v_\perp^2}{2}+v_\parallel^2\right)^2 QF_{0j}\left(\frac{\omega_{\mathrm{t}}/2}{\omega_{\mathrm{t}}^2/4-\omega^2}-\frac{3\omega_{\mathrm{t}}/2}{9\omega_{\mathrm{t}}^2/4-\omega^2}\right)_j \tag{12b}$$

Note that the core plasma finite Larmor radius effects appear through the parameter Δ_{K}. The magnitude of Δ_{K} indicates the relative importance of kinetic and fluid (toroidicity) effects in determining the regular mode structure of the various poloidal harmonics in the gap region [15]. Typically, one finds $\Delta_{\mathrm{K}} \lesssim 1$. The effect of the mode resonances with the core plasma particles is accounted for by the $\approx \beta_1$ and $\approx \beta_2$ terms [3]. In the long wavelength regime, $k_\vartheta\rho_{\mathrm{E}} \lesssim \epsilon_0$, the summation in Eqs (12a, b) is extended also to the energetic particles [3], and the $\approx \beta_1$ and $\approx \beta_2$ terms describe also the mode drive due to fast ions.

In Ref. [18], expressions were given for F_1, F_2 and F_3 in the TAE case, yielding $F_1 = \sqrt{-\hat{\Gamma}_+\hat{\Gamma}_-}$, $F_2 = (\hat{\Gamma}_+ + \hat{\Gamma}_-)/2$ and $F_3 = (\hat{\Gamma}_+ - \hat{\Gamma}_-)/2$. In the general case, these functions are computed from the large-θ solution of Eq. (4). The general forms for F_1, F_2 and F_3 are $F_1(\omega;\tau) = (A^{(-)}B^{(+)} - B^{(-)}A^{(+)})/2$, $F_2(\omega;\tau) = -(A^{(-)}A^{(+)} + B^{(-)}B^{(+)})/2$ and $F_3(\omega;\tau) = (A^{(-)}A^{(+)} - B^{(-)}B^{(+)})/2$. Expressions for $A^{(\pm)}$ and $B^{(\pm)}$ can be obtained either numerically or by using a WKBJ approach, yielding [9]

$$A^{(\pm)} = K^{(\pm)}\left(\frac{\Gamma(3/4-a/2)}{\sqrt{2\pi}(-a/2)^{-a/2+1/4}\mathrm{e}^{a/2}}\right)\sqrt{-\hat{\Gamma}_-}\left[\left(1+\frac{\Lambda}{2}\mathrm{e}^{-2T+2R}\right)+\mathrm{i}\mathrm{e}^{-2R}\left(1-\frac{\Lambda}{2}\mathrm{e}^{-2T+2R}\right)\right] \tag{13a}$$

$$B^{(\pm)} = \pm K^{(\pm)}\left(\frac{\Gamma(1/4-a/2)}{\sqrt{2\pi}(-a/2)^{-a/2-1/4}\mathrm{e}^{a/2}}\right)\sqrt{\hat{\Gamma}_+}\left[\left(1+\frac{\Lambda}{2}\mathrm{e}^{-2T+2R}\right)-\mathrm{i}\mathrm{e}^{-2R}\left(1-\frac{\Lambda}{2}\mathrm{e}^{-2T+2R}\right)\right] \tag{13b}$$

for $\mathrm{Re}\,\hat{\Gamma}_- \geq 0$,

$$A^{(\pm)} = K^{(\pm)}\left(\frac{\sqrt{2\pi}(a/2)^{a/2-1/4}\mathrm{e}^{-a/2}}{\Gamma(1/4+a/2)}\right)\sqrt{-\hat{\Gamma}_-}(1-\mathrm{i}\tilde{\Lambda}\mathrm{e}^{-2T}) \tag{14a}$$

$$B^{(\pm)} = \pm K^{(\pm)}\left(\frac{\sqrt{2\pi}(a/2)^{a/2+1/4}\mathrm{e}^{-a/2}}{\Gamma(3/4+a/2)}\right)\sqrt{\hat{\Gamma}_+}(1+\mathrm{i}\tilde{\Lambda}\mathrm{e}^{-2T}) \tag{14b}$$

for $\mathrm{Re}\,\hat{\Gamma}_- < 0$ and $\mathrm{Re}\,\hat{\Gamma}_+ \geq 1$,

$$A^{(\pm)} = K^{(\pm)}\left(\frac{\Gamma(1/4-a/2)}{\sqrt{2\pi}(-a/2)^{-a/2-1/4}\mathrm{e}^{a/2}}\right)\sqrt{-\hat{\Gamma}_-}\,(1-\mathrm{i}\mathrm{e}^{-2T}) \tag{15a}$$

$$B^{(\pm)} = \pm K^{(\pm)}\left(\frac{\Gamma(3/4-a/2)}{\sqrt{2\pi}(-a/2)^{-a/2+1/4}\mathrm{e}^{a/2}}\right)\sqrt{\hat{\Gamma}_+}\,(1+\mathrm{i}\mathrm{e}^{-2T}) \tag{15b}$$

for $\mathrm{Re}\,\hat{\Gamma}_- < 0$ and $0 < \mathrm{Re}\,\hat{\Gamma}_+ < 1$,

$$A^{(\pm)} = K^{(\pm)}\left(\frac{\sqrt{2\pi}(a/2)^{a/2+1/4}\mathrm{e}^{-a/2}}{\Gamma(3/4+a/2)}\right)\sqrt{-\hat{\Gamma}_-} \tag{16a}$$

$$B^{(\pm)} = \pm K^{(\pm)}\left(\frac{\sqrt{2\pi}(a/2)^{a/2-1/4}\mathrm{e}^{-a/2}}{\Gamma(1/4+a/2)}\right)\sqrt{\hat{\Gamma}_+} \tag{16b}$$

for $\mathrm{Re}\,\hat{\Gamma}_+ \leq 0$. In the above expressions, $\Gamma(z)$ is the Euler gamma function, and a, Λ, $\tilde{\Lambda}$, R and T have been defined as

$$a = -\hat{\Gamma}_+\hat{\Gamma}_-/2\sqrt{(\hat{\Gamma}_+ + \hat{\Gamma}_-)\Delta_\mathrm{K}}, \quad \Lambda = \sqrt{2\pi}\mathrm{e}^a(-a)^{-a}/\Gamma(1/2-a), \quad \tilde{\Lambda} = \Gamma(1/2+a)/\sqrt{2\pi}\mathrm{e}^{-a}a^a,$$

$$R = \int_0^{x_-}\sqrt{(\Delta_\mathrm{K}x^2 - \hat{\Gamma}_-)(\hat{\Gamma}_+ - \Delta_\mathrm{K}x^2)}\,\mathrm{d}x, \quad T = \int_0^{x_+}\sqrt{(\Delta_\mathrm{K}x^2 - \hat{\Gamma}_-)(\hat{\Gamma}_+ - \Delta_\mathrm{K}x^2)}\,\mathrm{d}x$$

with $x_\pm = \sqrt{\hat{\Gamma}_\pm/\Delta_\mathrm{K}}$. Equations (13a) to (16b) describe the coupling of toroidal Alfvén modes with kinetic Alfvén waves, including the so-called *radiative damping*. In the 'ideal' limit, $\Delta_\mathrm{K} \to 0$, the same expressions reduce to those previously derived for TAE modes [17, 18].

3. GLOBAL STABILITY ANALYSIS AND EIGENMODE STRUCTURES

Equation (7) embraces, in a non-perturbative way, equilibrium fluid and kinetic core plasma effects as well as energetic particle dynamics with finite orbit widths [9]. For this reason, it may be viewed as a unified description of TAEs, KTAEs and toroidal Alfvén energetic particle modes (EPMs) [9]. However, at the same time, it is difficult to handle analytically for a full 2-D global stability analysis that derives the mode frequency and the radial envelope function. For this reason, a numerical code has been developed, which determines the 'Stokes structure' of the complex τ plane associated with the local dispersion function, Eq. (7), and then finds the global eigenvalue by solving

$$\epsilon_\mathrm{T} n\left(\int_{r_1}^{r_2} q'(r)\theta_k(r)\,\mathrm{d}r + \theta_k(r_1)q(r_1) - \theta_k(r_2)q(r_2)\right) = (l+p)\pi \tag{17}$$

where, for convenience, a change of variable from τ to r has been performed, $\epsilon_\mathrm{T} = 1$ if $\theta_k(r_1) = 0$, $\epsilon_\mathrm{T} = -1$ if $\theta_k(r_1) = \pi$, and r_j are the (complex) radial WKBJ turning points, identified by the condition $\partial F(\omega;\tau,\theta_k)/\partial\theta_k = 0$ along with the local dispersion relation $F(\omega;\tau,\theta_k) = 0$. In Eq. (17), l is the radial mode number and $p = 1/2$ if the two turning points correspond to the same θ_k value, or $p = 0$ if they correspond to different θ_k.

Taking into account that, for up–down symmetric equilibria, WKBJ turning points occur at $(\theta_k = 0, \pi)$, the locations of the turning points are simply determined from the local dispersion relation, $F(\omega;\tau,\theta_k) = 0$, for a fixed value of ω and $\theta_k = 0, \pi$. For this purpose, a Stokes plot associated with Eq. (7) is drawn in the complex r plane. To solve Eq. (17), two turning points must be found but, in general, more than two will be present. The choice of the turning point pairs to be connected is dictated by the Stokes structure of the complex plane [9]. The phase integral in Eq. (17) is then evaluated by joining the selected turning points in the complex r plane along the path defined by $r = r_1 + (r_2 - r_1)t$, with the parameter t varying between 0 and 1. The global eigenvalue ω, in turn, is determined by evaluating the phase integral for five different values of ω and then using a five point interpolation scheme to obtain the value of ω for which Eq. (17) is satisfied. Such a procedure, iterated until convergence is reached, allows us to follow easily the various roots of the global dispersion relation when a characteristic equilibrium parameter is varied.

In our simple model, most of the computing time is used in the evaluation of the quantities Z_f, G_f, H_f and L_f. To this aim, the safety factor and the bulk-plasma pressure profiles are kept fixed and the quantities Z_f, G_f, H_f and L_f are evaluated on a grid in the complex r plane for real values of θ_k. The coefficients of the Fourier expansions in θ_k of Z_f, G_f, H_f and L_f are in turn determined and tabulated (note that they depend only on (s,α)). The analytic continuation of the expressions for Z_f, G_f, H_f and L_f in the complex θ_k plane together with an interpolation in the complex r plane is used to invert the local dispersion relation,

Eq. (7), and to determine numerically the WKBJ ray trajectories $\theta_k = \theta_k(r)$.

After having determined a global eigenvalue for which Eq. (17) is satisfied, a parameter such as the energetic particle density is varied keeping safety factor and bulk-plasma pressure profiles fixed (thus, not varying the s and α profiles). The previous solution is used as a guess for the new global eigenvalue ω. In this way, the dependence of global frequency spectra on relevant equilibrium parameters can be easily studied.

4. STABILITY OF TAE ON ITER

The code described above has been used to verify whether global Alfvén eigenmodes, such as TAE and KTAE, are unstable for ITER-like parameters. We will assume the following configuration as reference. The aspect ratio, minor radius and toroidal magnetic field are $A = 2.63$, $a = 2.3$ m and $B_0 = 5.7$ T, respectively. The temperature and density profiles are given by $n_e = n_0[1-(r/a)^2]^{\alpha_n}$ and $T = T_0[1-(r/a)^2]^{\alpha_T}$. In the following, we will assume that $T_0 = 20$ keV and $n_0 = 1.5 \times 10^{20}$ m^{-3}, $\alpha_n = 0.5$ and $\alpha_T = 1$ (thus the total bulk plasma β on axis is $\beta_{\text{bulk},0} \simeq 3.7\%$). The q profile is given by a parabolic profile with q on axis $q_0 = 1.0$ and q at the edge $q_a = 3.0$.

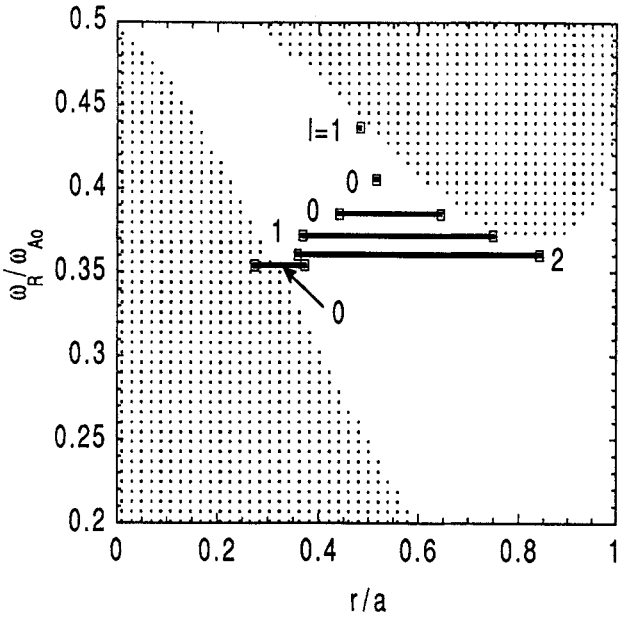

FIG. 1. Radial location of the turning points and real eigenvalues ω_R normalized to the Alfvén frequency in the centre ω_{A0}. Bulk and energetic-particle pressure effects as well as bulk electron and ion Landau damping are not included. The considered toroidal mode number is n = *10. The dotted area is the Alfvén continuum. The radial mode numbers* l *are also shown.*

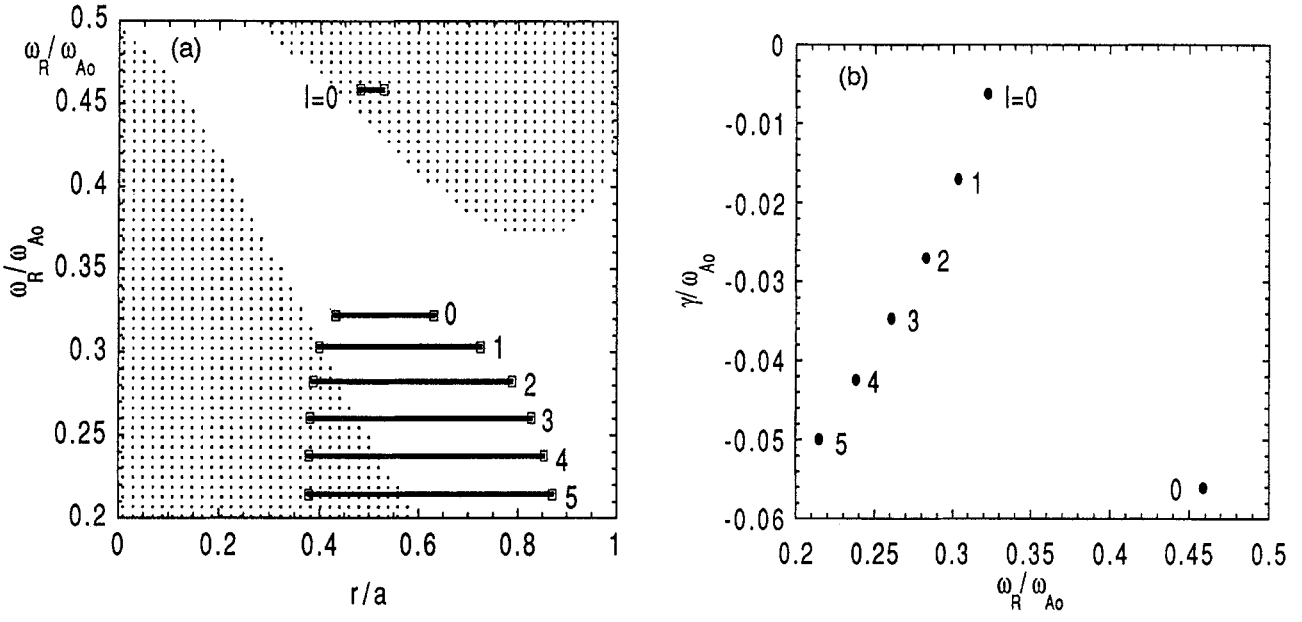

FIG. 2. (a) Radial location of the turning points and real eigenvalues ω_R/ω_{A0} for the same case as that of Fig. 1 except that now $\beta = \beta_{bulk}/2$. (b) The global frequency spectrum in the complex ω plane.

The alpha particle density, n_α, is evaluated from the condition $n_\alpha = \langle\sigma v\rangle n_{DT}^2/4\tau_{sd}$, $n_{DT} = n_e/2$, with $\tau_{sd}(s) = 1.2 \times 10^{-2} T_e(\text{keV})^{3/2}/n_e(10^{20}\ \text{m}^{-3})$, and $\langle\sigma v\rangle$ computed from the Peres expression [21]. This yields an alpha particle pressure profile given by $p_\alpha = p_{\alpha,0}[1 - (r/a)^2]^{\alpha_{hot}}$, with $\alpha_{hot} \simeq \alpha_n + 3.5\alpha_T$ and an alpha particle beta $\beta_{\alpha,0} \simeq 1.5\%$.

First, we will neglect the contribution of the energetic particles. In order to comment quantitatively on the importance of the bulk plasma β in determining the global stability properties of Alfvén modes, we will analyse three reference cases: $\beta = 0$, $\beta = \beta_{bulk}/2$ and $\beta = \beta_{bulk}$. Electron and ion Landau damping will also be neglected in this β parametric study. In this way, we will be able to show how the increase with β in the global mode damping is due to the stronger interaction (as β increases) with the lower Alfvén continuum [18, 19]. In Fig. 1 the radial location of the turning points and the real part of the eigenvalue spectrum for different TAE are shown for $\beta = 0$. The dotted regions indicate the Alfvén continuum. The toroidal mode number considered is $n = 10$. The thick lines connect the projection onto the real axis of the locations of the (complex) turning points r_1 and r_2. Neglecting radiative damping would result in eigenvalue and radial positions of the turning points being purely real quantities for the TAE branch and the upper KTAE branch. It has to be noted that the TAE modes are all located in the upper half of the frequency gap, because of the relatively large shear value [2]. In Fig. 2(a), the radial turning point location and the real part of the eigenvalue spectrum are shown for $\beta = \beta_{bulk}/2$. The finite-β effects shift the global mode frequencies toward the lower Alfvén continuum [18], transforming the TAE in mixed TAE/KTAE modes.

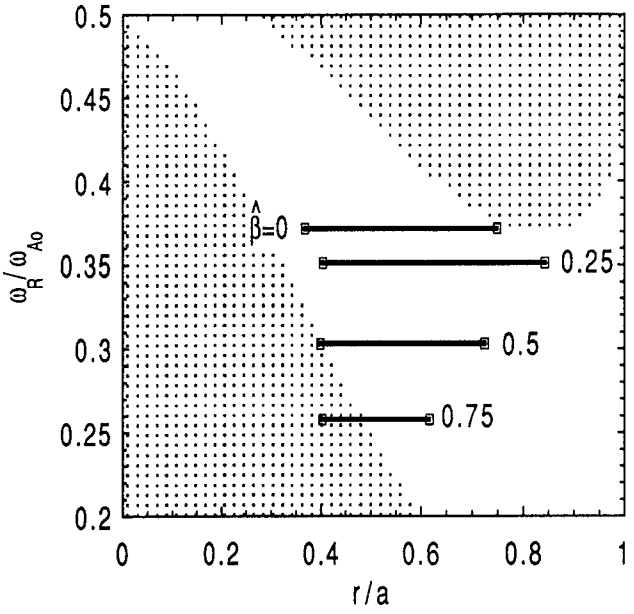

FIG. 3. Radial location of the turning points and real eigenvalues ω_R/ω_{A0} for the mode with radial mode number l = 1, as the normalized bulk-plasma $\hat{\beta} \equiv \beta/\beta_{bulk}$ is increased.

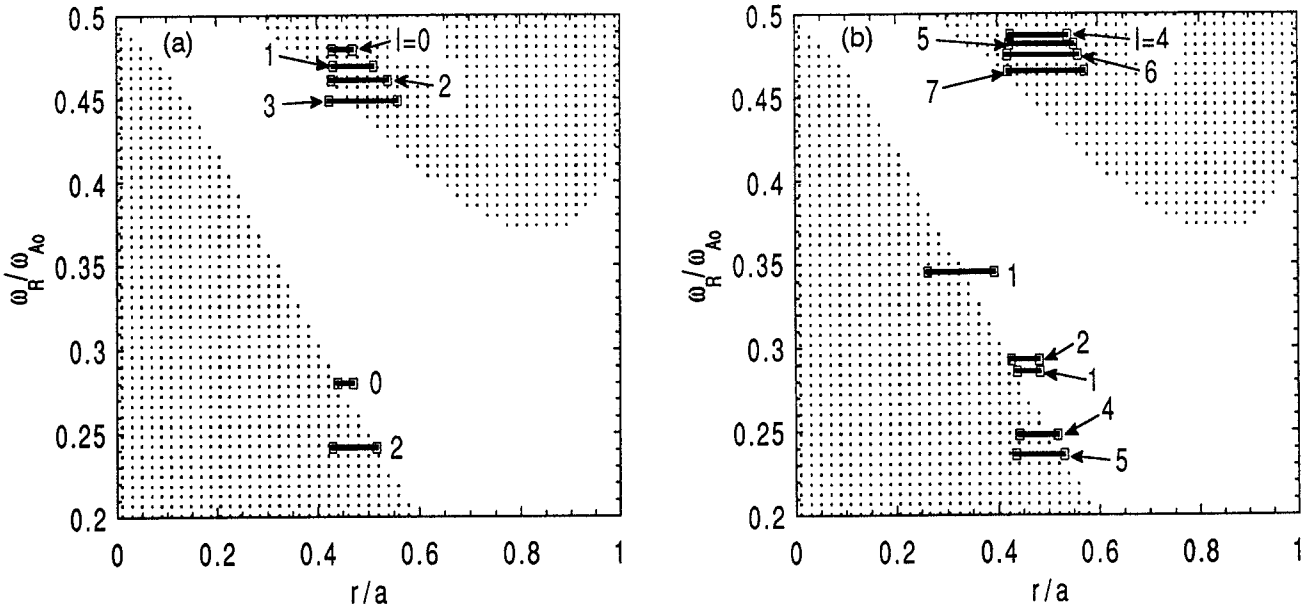

FIG. 4. Radial location of the turning points and real eigenvalues ω_R/ω_{A0} at the reference bulk-plasma $\beta = \beta_{bulk}$ for toroidal mode number (a) n = 10 and (b) n = 20.

In Fig. 2(b) the sequence of global TAE/KTAE eigenvalues is shown in the complex ω plane. Note that the global TAE/KTAE modes become more damped as their real frequency moves deeper into the Alfvén continuum. In Fig. 3 the radial turning point location and the real part of the mode frequency are shown for a particular global eigenmode (radial mode number $l = 1$) as the bulk plasma β is increased. Note how the finite-β effects shift the mode towards the lower continuum making it strongly damped for higher bulk-plasma β.

In Fig. 4 the radial localization and the real part of the global eigenvalue spectrum are shown, for the reference value $\beta = \beta_{\text{bulk}}$, and for two values of the toroidal mode number $n = 10$ (Fig. 4(a)) and $n = 20$ (Fig. 4(b)). Note that no pure TAE modes are present in the gap because of the finite-β_{bulk} effects. Only TAE/KTAE mixed modes are present in the upper and lower continua. These modes already suffer a considerable damping, in the absence of an alpha particle drive. Thus, we can foresee that their destabilization will be harder than in the presence of pure TAEs. This result confirms those of Ref. [9]; i.e. that ideal modes (TAEs) are the most unstable ones. If TAEs, for sufficiently high β_{bulk}, are caused to interact strongly with the lower Alfvén continuum and, thus, to be damped, only weak kinetic instabilities are left. In these conditions, strong instability can occur only for sufficiently high energetic particle drive. Then, the energetic particle continuum modes (EPMs) [9] are excited, but the analysis of these modes is beyond the scope of the present work.

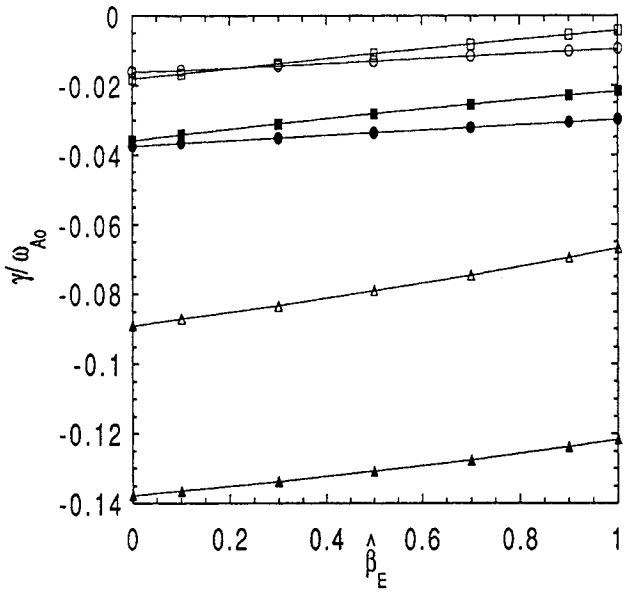

FIG. 5. Dependence of the growth (damping) rate on the normalized alpha particle beta $\hat{\beta}_E \equiv \beta_E/\beta_\alpha$, for an upper KTAE (circles) with n = *10,* l = *1, for an upper KTAE (squares) with* n = *20,* l = *4 and for a lower KTAE (triangles) with* n = *20,* l = *2. Open (filled) symbols refer to the bulk electron and ion Landau damping not included (included).*

Next, we consider the dependence of the global Alfvén spectrum on the alpha particle β, for a selected number of modes. In particular, an upper KTAE for $n = 10$ and an upper KTAE and a lower mixed TAE/KTAE mode for $n = 20$ have been chosen, to discuss the dependence of the eigenfrequency on β_{E}. In Fig. 5 the dependence of the eigenfrequencies on the alpha particle β is shown, with and without the bulk electron and ion Landau damping included. All the modes considered are shown to be stable, or at least very close to marginal stability. It has to be noted that the results obtained in this paper differ from those presented in Ref. [16], where a perturbative approach was considered for the relevant drive and damping terms. In Ref. [16] weakly unstable lower KTAEs were obtained for $n \geq 5$ and $\beta_{\text{E}} = \beta_\alpha$, but the conditions for the perturbative approach to be valid are easily violated for modes close to the Alfvén continuum, as already discussed in Refs [15, 16]. The conclusions about the results presented in this paper and those in Ref. [16] about ITER-like equilibrium are nevertheless not significantly different, the considered modes being close to marginality in both cases. Note that this does not need to be the general case. Scenarios can be envisaged in which non-perturbative analyses lead to dramatically different conclusions, for example, the prediction of a completely new EPM [9].

As a general consideration, the modes with higher toroidal mode number tend to be less stable (or more unstable) (in fact, the driving term related to the energetic particles is proportional to $\omega_* \propto k_\theta \propto n$).

5. CONCLUSIONS

As a conclusion, we want to note that for the first time a code that solves the 2-D mode structure and global stability of Alfvén branches has been presented. It uses a local dispersion relation that, in general, can be obtained numerically or analytically. In the present paper, a local dispersion relation obtained from the two spatial-scale WKBJ formalism without employing perturbation theory in the treatment of drive and damping terms has been used.

Generally speaking, two different scenarios are foreseen to be dangerous for ITER. The first scenario is the one in which ideal fluid modes (TAEs) are present inside the continuum gap: in fact, finite-β_E effects can easily drive these modes unstable. From the preliminary analysis presented in the previous section this is not the case for the reference ITER configuration ($T_0 = 20$ keV, $n_0 = 1.5 \times 10^{20}$ m^{-3}), as the finite-β_{bulk} effects shift the modes outside the continuum gap towards the (lower) Alfvén continuum. The second scenario is the one in which the toroidal Alfvén EPMs [9] are driven unstable by sufficiently high β_E. Again, the reference ITER configuration has too low a β_E to drive these modes unstable. Thus, ITER seems to be in an intermediate situation, where only a variety of kinetic modes are present (see Fig. 4), which are stable or close to marginal stability. In such a scenario, small changes in equilibrium profiles can modify the stability properties of the Alfvén spectrum. Moreover, non-perturbative analyses are required in such a case. In fact, treating the kinetic effects perturbatively [16] predicts global unstable KTAE spectra for $n \geq 5$, whereas a fully non-perturbative treatment, as done in the present paper, results in the mixed TAE/KTAE modes being stable.

In the near future, this preliminary analysis for the ITER scenario will be completed and applications to the TFTR DT shots will also be considered.

REFERENCES

[1] KIERAS, C.E., TATARONIS, J.A., J. Plasma Phys. **28** (1982) 395.

[2] CHENG, C.Z., et al., Ann. Phys. (N.Y.) **161** (1985) 21.

[3] CHEN, L., in Theory of Fusion Plasmas (Proc. Course Joint Varenna–Lausanne Int. Workshop Chexbres, 1988), Editrice Compositori, Bologna (1988) 327.

[4] BETTI, R., FREIDBERG, J.P., Phys. Fluids B **4** (1992) 1465.

[5] MAZUR, V.A., MIKHAJLOVSKIJ, A.B., Nucl. Fusion **17** (1977) 193.

[6] GORELENKOV, N.N., SHARAPOV, S.E., Phys. Scr. **45** (1992) 163.

[7] TSAI, S.T., CHEN, L., Phys. Fluids B **5** (1993) 3284.

[8] CHEN, L., Phys. Plasmas **1** (1994) 1519.

[9] ZONCA, F., CHEN, L., Bull. Am. Phys. Soc. **39** (1994) 1701;
ZONCA, F., CHEN, L., Theory of toroidal Alfvén modes excited by energetic particles in tokamaks, Phys. Plasmas (in press).

[10] BERK, H.L., et al., Phys. Lett. A **162** (1992) 475.

[11] FU, G.Y., CHENG, C.Z., Phys. Fluids B **4** (1992) 3722.

[12] CANDY, J., ROSENBLUTH, M.N., Phys. Plasmas **1** (1994) 356.

[13] METT, R.R., MAHAJAN, S.M., Phys. Fluids B **4** (1992) 2885.

[14] CANDY, J., ROSENBLUTH, M.N., Plasma Phys. Control. Fusion **35** (1993) 957.

[15] ZONCA, F., Plasma Phys. Control. Fusion **35** (1993) B307.

[16] ROMANELLI, F., ZONCA, F., in Tokamak Concept Improvement (Proc. Workshop Varenna, 1994), Editrice Compositori, Bologna (1994) 191.

[17] ZONCA, F., CHEN, L., Phys. Rev. Lett. **68** (1992) 592.

[18] ZONCA, F., CHEN, L., Phys. Fluids B **5** (1993) 3668.

[19] ZONCA, F., Continuum Damping of Toroidal Alfvén Eigenmodes in Finite-Beta Tokamak Equilibria, PhD Thesis, Princeton Plasma Phys. Lab., Princeton, NJ (1993).

[20] CONNOR, J.W., et al., Phys. Rev. Lett. **40** (1978) 396.

[21] PEREZ, A., J. Appl. Phys. **50** (1979) 5569.

(Manuscript received 1 June 1995
Final manuscript accepted 5 September 1995)